

1 **Role of pressure solution in the formation of bedding-** 2 **parallel calcite veins in an immature shale (Cretaceous,** 3 **southern UK)**

4 **QINGFENG MENG, JOHN HOOKER & JOE CARTWRIGHT**

5 Department of Earth Sciences, University of Oxford, South Parks Road, Oxford, OX1 3AN, UK

6 Correspondence author. Email address: meng.qingfeng@hotmail.com

7 **Abstract:** Bedding-parallel fibrous calcite veins in black shales (Cretaceous, southern UK) were
8 investigated using a combined field, stable isotopic geochemistry, petrographic and
9 crystallographic method, to examine their formation mechanism. Calcite veins occur in all shale
10 beds and are most abundant in the bituminous shales of the Chief Beef Beds. The calcite fibres in
11 these veins exhibit either an antitaxial fibre growth with curvy stylolites as the median zone, or a
12 predominantly syntaxial, upward growth. The calcite veins range from -0.49 to 1.78‰ of $\delta^{13}\text{C}$
13 values, and -6.53 to -0.03‰ of $\delta^{18}\text{O}$ values, which are both similar to those of their host shales.
14 Our petrographic observations demonstrate that sub-horizontal and interconnecting microstylolite
15 networks commonly occur within the calcite veins. Equant calcite grains in the median zones
16 exhibit indenting, truncating and also interpenetrating grain contacts. It is interpreted that the
17 fibrous calcite veins were sourced by neomorphic calcite from their host shales, with evidence
18 from the $\delta^{13}\text{C}$ signatures, pressure solution features (stylolites, microstylolites and grain contact
19 styles), and embedded fossil ghosts within the veins. The diagenetic fluids, from which calcite was
20 precipitated, were a mixing of the original seawaters and ^{18}O -depleted meteoric waters.

Development of bedding-parallel calcite veins is considered to have been enhanced by pressure solution as a positive feedback mechanism, which was facilitated by the overburden pressure as the maximum principal stress. Calcite fibres, with a predominant subvertical c-axis orientation, exhibit a displacive growth in porous shales, and a replacive growth at vein-limestone contacts. This study highlights the critical role of pressure solution in the formation of bedding-parallel calcite veins during burial and diagenesis of immature black shales.

Keywords: pressure solution; bedding-parallel; beef; stylolite; shale; c-axis

1. Introduction

Pressure solution is a deformation process by which grains dissolve at intergranular or intercrystalline contacts under high stress in an aqueous solution (Thomson, 1959; Weyl, 1959; Rutter and Elliott, 1976; Fletcher and Pollard, 1981; Rutter, 1983; Tada and Siever, 1989). Such a process is caused by a higher solubility under nonhydrostatic stresses at grain-to-grain contacts. Two common types of pressure solution have been recognized: intergranular pressure solution and stylolitization (Houseknecht, 1984; Tada and Siever, 1989; Dewers and Ortoleva, 1990; Bjorkum, 1996). Intergranular pressure solution, as a diagenetic mechanism, contributes significantly to porosity reduction and compaction, serving as the agent of intergranular compaction and a source of cement (e.g. Sibley and Blatt, 1976; Houseknecht, 1984, 1988; Tada et al., 1987; Lehner, 1995; Renard et al., 1997; Renard et al., 2000; Yasuhara et al., 2003). Stylolites can be recognized by serrated surfaces within the rock mass, where insoluble minerals, such as clay, iron minerals and organic matter, are concentrated (Park and Schot, 1968). Based on their morphology, stylolites can be subdivided into several types with varied amplitudes of offset, column frequency, peak angles, orientations and connectivities (Fig. 1) (Koehn et al., 2016). Stylolites has been regarded as an important cement source, especially for late diagenetic calcite spar (Oldershaw and Scoffin, 1967;

Finkel and Wilkinson, 1990; Rezaee and Tingate, 1997; Worden et al., 1998; Baron and Parnell, 2007; Koehn et al., 2016). Stylolites can prevent fluid flow (Heap et al., 2014), whereas in other settings, serve as conduits for fluid flow (Carozzi and Von Bergen, 1987; Braithwaite, 1989).

It has been recognized that bedding-parallel fibrous veins (or “beef”) are common in black shales in sedimentary basins worldwide, where they are often taken an example for high pore fluid pressures (Cobbold et al., 2013). The characteristic feature of such veins is that they consist of parallel-aligned crystals with a maximum length of several centimeters, and exhibit a fibrous texture (Bons, 2000; Bons et al., 2012). Multiple mechanisms have been proposed to explain the genesis of these veins (Table 1); however, the debate still remains. The key questions to discuss mainly include (1) the mechanism that triggered the initiation of bedding-parallel veins; and (2) the origin of the fibrous habit of crystals and the driving force for vein expansion.

In this paper, we report a field, isotopic, petrographic and crystallographic study of the bedding-parallel calcite veins in the Stair Hole Member exposed in Dorset, southern UK. The work extends the original study of El-Shahat and West (1983) on the diagenesis of the Purbeck Formation by carrying out a more thorough investigation of the calcite veins, regarding their stratigraphic distribution, morphology, size, stable isotope geochemistry, petrography and c-axis crystallography. This paper aims to provide new evidence for (1) the diagenetic environment for fibrous calcite veins; (2) the vein formation mechanism; and (3) the mutual interplay between vein fabrics and their growth processes. The results presented in this study suggest that there is a positive feedback between pressure solution and the development of bedding-parallel calcite veins during chemical compaction of the host fossiliferous sediments, when the thermal maturity of organic matter is not high enough to generate hydrocarbons. This study also raises the important

possibility that the classical views regarding formation mechanism of bedding-parallel veins in shale may need to be restricted.

2. Geological background

The study area is located on the coastal area of the Durlstone Bay, Dorset, southern UK (Fig 2a). The cliffs expose 119 m thick alternating limestones and shales of the Purbeck Group (Upper Jurassic – Lower Cretaceous) (Fig. 2b, c). The beds are NWW-SEE-striking and gently dipping towards north at ten degrees. The lower boundary of the Purbeck is defined by the first occurrence of finely laminated, ostracod-rich limestones above the more massive, shelly limestones of the Portland Group (Horton, 1995). The overlying Wealden Group can be identified by the occurrence of sandy mudstones above the last occurrence of limestones of the Purbeck Group (Stewart et al., 1991; Robinson and Hesselbo, 2004). The thin-bedded limestones and calcareous shales of the Purbeck Group have been considered as lagoonal deposits, which are richly fossiliferous, especially bivalves (Andrews and Walton, 1990; Stewart et al., 1991; Radley et al., 1998). There have been multiple rapid salinity fluctuations of the Purbeck Group. This is represented by a progressive change from strata with evaporites of hypersaline origin in the lower Purbeck to alternating freshwater, brackish and marine strata in the middle Purbeck to dominantly freshwater with influx of land-derived clastics in the upper Purbeck (Stewart et al., 1991; Schnyder et al., 2006; Radley, 2009). The middle part of the Purbeck Group has been extensively studied because the unlithified shell limestones are best developed within this interval (El-Shahat and West, 1983; Clements, 1993; Westhead and Mather, 1996). The most common bivalve deposits of the Purbeck Group consist of disarticulated valves of brackish-water bivalves. The unlithified shell beds typically contain white aragonite shells, whereas the lithified shell beds are composed of biosparites or biosparrudites with varying content of aragonite retained (El-Shahat and West, 1983). Bedding-parallel calcite veins

are commonly present in the Stair Hole Formation of the middle part of the Purbeck Group (El-Shahat and West, 1983; Westhead and Mather, 1996). The Stair Hole Formation can be further subdivided into five beds with different lithologies and degrees of lithifications (Fig. 2b) (Westhead and Mather, 1996).

3. Methods

An integrated research method of field, optical and SEM petrography and crystallography, and stable isotope geochemistry was used to study the bedding-parallel veins. Field investigation mainly focused on the distribution, geometry and abundance of calcite veins and their host rock lithologies. Calcite veins and their host rocks were sampled for carbon and oxygen isotope measurements, to derive information of the carbonate source, diagenetic fluid and environment. The measurements were conducted using Thermo MAT 253 mass spectrometers at the Stable Isotope Geochemistry Laboratory of Open University, following the procedure described by Meng et al. (2017a). Oxygen ($\delta^{18}\text{O}$) and carbon ($\delta^{13}\text{C}$) isotopes were obtained at precision better than ± 0.06 and ± 0.05 , respectively. Thin sections of representative rock samples of calcite veins and surrounding rocks were cut perpendicular to bedding. We used a polarized light microscope and a FEI Quanta 650 scanning electron microscope (SEM) to observe vein microstructures, mineral compositions and diagenetic alternations of the host rocks. We also used EBSD technique to quantitatively measure crystallographic preferred orientations (CPO) (Humphreys, 2004) and sizes of calcite crystals in the vein samples, so that the information of crystal growth and paleostress states could be revealed (Meng et al., 2018). The polished thin sections were mounted on a tilted SEM stage at 70° from horizontal, with the vein walls being parallel to the x-axis of the stage. The measurement was conducted at 20 kV accelerating voltage, and a working distance of 10 mm from the EBSD detector. Electron beam scattering patterns were automatically collected using the Aztec

software package for identification of the crystal orientations. The microstructural maps were then generated to spatially describe the crystal lattice orientations. The c-axis orientations of some selected crystals were plotted as lower-hemisphere, equal-area stereographic projections using the HKL Channel 5 software, which allows a comparison between these crystals.

4. Field observations

4.a. Vein distribution

Bedding-parallel, fibrous calcite veins were found in all the shale-containing beds of the Stair Hole Formation, except the Scallop Bed (Table 2). Fibrous calcite veins are prevalent in the Chief Beef Beds, occurring in every shale bed. They are most abundant in Bed 219 (Fig. 3a - e), which consists of 55 cm thick, bituminous shales. The shales are rich in iron and original skeletal aragonite. The bedding-parallel veins are intensively developed and tightly clustered. 55 veins occur along a linear scanline normal to bedding, with an average spacing of 6.35 mm (spacing is here defined as the thickness of shale between two neighboring veins) (Fig. 4). Vein sizes vary from 0.2 - 2.8 cm in thickness, and 1 - 2 cm to tens of meters in length. Other shale beds of the Chief Beef Bed contains only one or two calcite veins (Fig. 3f - i). The veins lie either in the central part of the beds, or more commonly close to the neighbouring limestone beds (< 10 cm). For example, two veins in Beds 205 and 207 were found to bound their host shales and a limestone bed (Bed 206) (Fig. 3g).

Persistent bedding-parallel calcite veins with a maximum thickness of 1.3 cm were observed in Beds 160 and 164 of the Corbula Bed (Fig. 3h, i). These beds also contains abundant aragonitic bivalves and gastropods, which has not been lithified. Bed 130, as the only shale bed of the Intermarine Bed, consists of a 1.5 cm thick calcite vein and prevalent shell debris. Three to four closely-spaced calcite veins were found at the more argillaceous, uppermost part of the Cinder Bed

(Bed 111), which contains bluish, grey shelly limestone with oysters. The veins are persistent in length and vary from 2 to 5 mm in thickness.

4.b. Morphology

The calcite veins are either tabular shaped and persistent in length, or are spindle-shaped with conspicuous tips (Fig. 3c). Some vein tips are sharply tapering, whereas many others exhibit blunt or even rounded tips (Fig. 3d). The veins consist of closely-packed vertical fibres, which are approximately normal to vein-walls. Some calcite veins contain a median zone that bounds the upper and lower fibres (Fig. 3f). The median zones are either straight or curvy, and are mostly nearer to the lower vein-walls, i.e. the upper fibres are predominantly longer than the lower fibres. The curvy median zones exhibit characteristic features of stylolites (Fig. 3c), with a maximum column amplitude of 8 mm. The crowns of individual columns are commonly curvy, and the peaks are rather blunt. Three-dimensional shapes of stylolites are occasionally weathered out, exposing a forest of columns and matching pits normal to the planes of the stylolites. Median zones are commonly absent in many calcite veins (Fig. 3g). In such veins, calcite fibres become coarser towards the upper vein-walls, exhibiting a syntaxial, upward growth.

Vein surfaces are commonly irregular. The rugosity of vein planes can be attributed to the variable degrees of fibre protrusions into the host rocks. For example, the uppermost calcite vein of Bed 219 (Chief Beef) with rough planes results in the corresponding irregularity in the contact with the limestone of Bed 220 (Broken Shell) (Fig. 5a). This demonstrates that the longer fibres in the vein have protruded into the limestone, causing a differential compaction of the limestone. It is also observed that thin calcite veins at the top of the Cinder Bed contain numerous bivalve residues on vein surfaces (Fig. 5b). The fossil morphologies are rather intact, which contributes to the irregular surface geometry of vein planes.

5. Stable isotope signatures

The $\delta^{13}\text{C}$ values of the calcite veins from the Chief Beef Bed vary from -0.49 to 1.78‰ PDB (Fig. 6). Coupled with their $\delta^{18}\text{O}$ compositions, the veins can be subdivided into two groups (Fig. 7). Veins of group I mostly occur in the upper part of this bed and exhibit positive $\delta^{13}\text{C}$ values ranging from 1.11 to 1.78‰ PDB. Group II are located in the lower part of this bed and have negative values ranging from -0.49 to -0.30‰ PDB. The $\delta^{18}\text{O}$ values of both groups are between -6.74 to -5.47‰ PDB, and are generally overlapped and undifferentiable.

The limestones of the Chief Beef Bed exhibit varied stable isotope compositions, -0.90 to 1.85‰ PDB of $\delta^{13}\text{C}$ values, and -6.53 to -0.03‰ PDB of $\delta^{18}\text{O}$ values (Fig. 6). The $\delta^{13}\text{C}$ compositions of the limestones are similar to those of calcite veins; however, their $\delta^{18}\text{O}$ compositions cross a much wider range. The anomalies of $\delta^{18}\text{O}$ values occur in Beds 192, 194 and 198, which all consist of unlithified aragonitic bivalves, with $\delta^{18}\text{O}$ values ranging from -0.54 to -0.03‰ PDB. The limestone beds with $\delta^{18}\text{O}$ values from -4.00 to -3.00‰ PDB consist of ostracod biosparite limestone. The biosparrudite limestone beds fall into a narrow range of $\delta^{18}\text{O}$ values from -5.15 to -5.37‰ PDB. The $\delta^{18}\text{O}$ values of other types of limestones are overlapped between -6.53 to -4.43‰ PDB.

The shale beds of the Chief Beef Bed exhibit a narrower range of stable isotope compositions than the limestone beds, with $\delta^{13}\text{C}$ values between -0.18 and 1.61‰ PDB, and $\delta^{18}\text{O}$ values between -5.86 and -2.18‰ PDB. An anomaly appears in Bed 193, which are neighbouring to two unlithified bivalve beds and exhibits a less negative $\delta^{18}\text{O}$ of -2.18‰ PDB.

The other calcite vein samples from the Corbula, Intermarine and Cinder Beds all have positive $\delta^{13}\text{C}$ values ranging from 0 to 1‰ PDB, and $\delta^{18}\text{O}$ values ranging from -6 to -5‰ PDB. It is notable that the calcite veins from the Cinder Bed exhibit higher $\delta^{13}\text{C}$ and lower $\delta^{18}\text{O}$ values than those of their host rocks (Fig. 8).

6. Petrography

6.a. Microtextures

The curvy median zones of stylolites in individual calcite veins consists of multiple columns with a height ranging from 0.2 to 2.1 mm, and a frequency of 0.7/mm (Fig. 9). The stylolites mainly contain insoluble clay minerals, organic matter and pyrite microcrystals. The thickness of the stylolites varies from several microns to 0.6 mm. The original structure of fine laminations has largely been retained (Fig. 9b, c), which are parallel to the contacting flanks of columns. Plastic deformation and shear fractures commonly occur in the clay aggregates.

Calcite occurs in two major forms in the veins, either as equant, small crystals, or as larger fibres with a much higher aspect (length/width) ratio. Here, small crystals are defined as those with an area size less than $10^4 \mu\text{m}^2$. The small calcite crystals are predominantly concentrated along the stylolites, especially at the crowns of individual columns. These crystals have an average size area of $2368 \mu\text{m}^2$, and an average aspect ratio of 3.3. The larger calcite crystals have an average size area of $29,443 \mu\text{m}^2$, and an average aspect ratio of 7.0, indicating that larger crystals tend to exhibit a lenticular or fibrous morphology. The calcite fibres are parallel, tightly aligned with the long axes lying vertically. The lower part of single veins are generally pure in composition, whereas the upper part contains numerous scattered inclusion patches of clay grains, pyrite and also organic matter. The upper walls of the veins also often exhibit a higher irregularity than the lower walls (Fig. 9a).

Ghosts of bivalve fragments are commonly observed to be embedded within the fibrous veins (Fig. 9d, e). The bivalve fragments are commonly flat or curved. Their length ranges from 20 to $150 \mu\text{m}$, and thickness from 1 to $4 \mu\text{m}$. The bivalve fragments mostly lie parallel to bedding; however, some fragments are oblique to bedding at an angle up to 55 degrees. Clay aggregates are commonly

associated with the bivalve fragments. The clay aggregates, with a thickness of 5 to 80 μm , predominantly lie below the bivalve fragments. Fibrous calcite crystals, which lie above the bivalve fragments, are rooted in the fragments, with little host-rock inclusions between them.

Crystalline mosaic of small, equant calcite crystals were also found filling the moulds of skeletal fragments as sparry calcite cement (Fig. 10). The crystal morphologies are similar to those in the stylolites of fibrous veins. Individual crystals are discernable with the long dimension ranging from 5 to 300 μm . The morphologies of the fragments are well retained. This is possibly because the cementation process predates mechanical compaction, so that crushing of the shell fragments has been avoided. Such sparry calcite cements have been suggested to be the result of neomorphism of aragonite during diagenesis, and an important origin of porosity reduction (El-Shahat and West, 1983).

6.b. Microstylolites

Microstylolites are commonly observed in the calcite veins, and truncate calcite crystals (Fig. 11). These microstylolites can be identified by wavy seams of organic matter with a maximum thickness of 22 μm (Fig. 11a, b). The microstylolites are generally sub-horizontal; however, most veins contain inclined or even vertical segments. Some microstylolites occur as interconnecting networks, consisting of multiple stylolites in varying orientations that do not cross-cut each other (Fig. 11c, d). These microstylolite networks mainly appear in closely-packed aggregates of relatively small crystals with insoluble inclusions along crystal boundaries, exhibiting a fitted fabric. Unlike macro stylolites, single microstylolites either have sharp peaks, or are composites of wavy or rectangular fragments with minor jagged surfaces. The amplitude of single columns ranges from 1 to 115 μm .

6.c. Grain contacts

The small, equant calcite grains within the calcite veins have different shapes and radius. Neighbouring grains in contact exhibit grain surface solution textures (Fig. 11e, f). The grains with small radius of curvature commonly penetrate into the grain with the larger radius of curvature, resulting in an indenting grain contact as the most common type of grain contacts. Neighbouring grains with similar radii often exhibit flat contacts, which is identified as truncating grain contacts. Interpenetrating grain contacts, i.e. mutually interlocking protrusions of grains into each other, were also observed. The sutured grain boundaries exhibit a similar morphology to microstylolites. By contrast to the equant grains, the vertical calcite fibres predominantly have smooth fibre boundaries, lacking signs of grain surface solution textures (Fig. 11f).

6.d. Deformation twins

Intracrystalline deformation by twinning was observed to be concentrated along the stylolites in the calcite veins (Fig. 12). The deformation twins gradually disappear towards vein walls. This suggests that the twins formed during the early stage of fibre growth as growth twins rather than deformation twins formed due to the loading of tectonic stress. Otherwise, the distribution of twins would be expected to be more homogeneously distributed within the veins. The twin sets often exhibit an interfingering pattern. Because the maximum principal stress σ_1 is ideally at about 45 degrees to the glide plane (Lacombe, 2010; Fossen, 2016), the interfingering twins suggest a subvertical σ_1 that was responsible for creating those twins.

7. C-axis fabrics

EBSD results demonstrate that the equant calcite crystals along the stylolites predominantly exhibit random c-axis orientations (Fig. 13a - c), whereas the much larger fibres exhibit a preferred c-axis orientation in the sub-vertical direction (Fig. 13a, b and d). Some fibres with a medium plunge, e.g. fibre 4 and 5 in Fig. 13a, are commonly overgrown by neighbouring fibres. Those

fibres have a tapering tip pointing towards vein walls. The steeply-plunging calcite fibres tend to have a constant crystal width during growth, which is greater than low - medium plunging calcite fibres or equant grains. In contrast to the fibres, the sparry calcite cement filling skeletal fragments exhibit random c-axis orientations, and similar crystal sizes to those in vein stylolites (Fig. 10b).

8. Discussion

8.a. Diagenetic environment

Previous studies have demonstrated that local dissolution of bioclasts ($\delta^{13}\text{C} \approx 0\text{‰}$) could provide carbonate for the precipitation of calcite in veins (Marshall, 1982; Wolff et al., 1992; Meng et al., 2017a). The carbon isotope values of bedding-parallel calcite veins (-0.5 to 1.8‰) presented in this study fall within a similar range to those of their host rocks (Figs. 6 - 8). The approximately equal values of $\delta^{13}\text{C}$ of calcite veins, shales and limestones could then suggest that the veins largely derived carbonates from the surrounding rocks. The calcite source could be neomorphic calcite provided by aragonitic fossils, or sparry calcite cements filling pore spaces, or a combination of both. The prevalent aragonitic shells in the limestone and shale beds of the Stair Hole Formation, especially those embedded on vein surfaces and also within the veins (Figs. 5b, c, 9d, e), could have released abundant carbonate for the growth of adjacent veins. This is because aragonite, as a more soluble polymorph of calcium carbonate, is metastable and readily to transform to calcite during burial (Maliva and Dickson, 1992; Hendry et al., 1995). In particular, the calcite veins and their host shales in beds 191, 193, 205, 215 and 219 share similar ranges of $\delta^{13}\text{C}$ values, suggesting that the veins were self-sourced by their host shales. It is notable that the unlithified aragonitic shell beds exhibit relatively more positive carbon isotope compositions, e.g. beds 194, 198 and 206 (Fig. 6). This could help explain the higher $\delta^{13}\text{C}$ values of calcite veins in shale beds 205, 215

and 219, because the carbonate mineralogy in these beds predominantly consists of unlithified skeletal aragonite as the carbonate source for the calcite veins in the beds.

Organically derived bicarbonate with depleted ^{13}C ($\delta^{13}\text{C} \approx -25\text{‰ PDB}$) has been suggested as an alternative source for calcite veins, through in-situ decomposition of organic matter under sulphate-reducing conditions (Hudson, 1978; McLane, 1995). Although the dark shales in the Stair Hole Formation is organic rich, the carbon isotope compositions of the calcite veins are not compatible with those infilled with organically-derived carbonate. Moreover, the calcite veins presented in this study are mainly composed of ferroan calcite (El-Shahat and West, 1983), similar to that of neighbouring compacted biosparrudite. Ferroan calcite could not have been readily precipitated whilst SO_4^{2-} was present and transformed to S^{2-} and H_2S , indicating that the precipitation of ferrous calcite for the calcite veins and calcite cements of the compacted biosparrudite postdated the process of bacterial sulphate reduction.

The oxygen isotope composition of carbonates is a function of the isotope composition and temperature of the water in which the carbonate minerals were precipitated (Boggs, 2009). This relationship is determined by:

$$T(^{\circ}\text{C}) = 16.9 - 4.2(\delta_c - \delta_w) + 0.13(\delta_c - \delta_w)^2 \quad (1)$$

Where δ_c is the equilibrium oxygen isotope composition of calcite; δ_w is the oxygen composition of the water from which the calcite was precipitated. Hence, the oxygen isotope composition becomes more negative as the burial depth and temperature increases. The $\delta^{18}\text{O}$ values of the unlithified aragonitic shell beds 194 and 198 are $\sim 0\text{‰ PDB}$ (Fig. 6), suggesting that the seawater had an original oxygen isotope composition of approximately zero per mill. If we assume that the diagenetic fluids for the calcite veins only consist of original seawater, using equation 1, the result of calculation of the formation temperature of the calcite veins would be around 52.3 to 53.2°C,

when given a $\delta^{18}\text{O}$ value of -5 to -6‰ PDB. However, the calculated temperatures are too high to be compatible with the palaeotemperatures indicators of apatite fission track and vitrinite reflectance data reported in previous studies (Fig. 14) (Bray et al., 1998; Greenhalgh, 2016). This indicates that the diagenetic fluids from which calcite was precipitated could have more negative oxygen isotope compositions, and contains ^{18}O -depleted water constituents. Such water constituents are mostly likely isotopically light meteoric waters, because it has been suggested that the precipitation of ferroan calcite cement for the compacted biosparrudites, which exhibit similar oxygen isotope ranges to the calcite veins, occurred as a typical phreatic process (Richter and Fuchtbauer, 1978). The mixing of seawater and isotopically light meteoric waters would affect the overall $\delta^{18}\text{O}$ signatures of the calcite precipitates. It may also be likely that evaporation have occurred and caused a heavier isotope composition, however, this effect can be in a deep environment and also a closed system.

In summary, the bedding-parallel calcite veins were mainly sourced by the host shales during burial, and postdates bacterial sulphate reduction. Calcite was precipitated from pore waters, which were a mixing of the original seawater and ^{18}O -depleted meteoric waters.

8.b. Vein generation and the paleostress states

The stylolites (Figs. 3b, c and 9a), microstylolites (Figs. 11a - d) and grain contact styles (Fig. 11e - f) found within the calcite veins suggest that pressure solution commenced during chemical compaction of their host sediments. The onset of chemical compaction has been suggested to occur between 200 to 1500 m (Boggs, 2009; Goult et al., 2012). Based on the burial history of the Durlstone Formation (Fig. 14), it is suggested that the calcite veins formed during burial and diagenesis, i.e. chemical compaction, of the host sediments. Coupled with evidence from the predominant horizontal directions of stylolites and the interfingering twins in the calcite fibres (Fig.

12), it could be inferred that the compressional stress leading to pressure solution is the gravitational stress due to the overburden load.

The small, equant calcite crystals along the stylolites within calcite veins (Figs. 11e, f and 13a) are similar to the sparry calcite filling shell moulds (Fig. 10), regarding crystal morphologies, sizes, crystallographic orientations and contact styles. Given the common co-existence of ghosts of bivalve fragments (Fig. 9d, e), those equant calcite in veins are interpreted to result from neomorphism of skeletal aragonite. The stylolites, as the vein initiation sites, could have formed due to pressure solution of neomorphic calcite within the horizons where aragonitic shells are concentrated, when the neomorphic calcite grains became large enough to get contact with neighboring grains. The stylolites are generally lying in the horizontal direction with columns aligned vertically due to the vertical overburden pressure.

The most commonly advocated mechanism to explain the genesis of fibrous calcite veins is that of overpressure triggered by primary oil migration from thermally matured organic matter (Stoneley, 1983; Parnell and Carey, 1995; Parnell et al., 2000; Cobbold and Rodrigues, 2007; Rodrigues et al., 2009; Zanella et al., 2015; Hooker et al., 2017). This is theoretically possible because (1) fluid pressure can hold apart fracture walls, and create dilational sites for the precipitation of calcite crystals when fluid pressure exceeds the sum of the minimum principal stress and the tensile strength of the shales (Stoneley, 1983); and (2) liquid oil have been observed within fluid inclusions in horizontal calcite veins (e.g. Parnell et al., 1996; Parnell et al., 2000). However, this mechanism is considered unlikely for the fibrous veins of the Stair Hole Member for a number of reasons.

Firstly, it has been suggested that the black shales of the Cretaceous as well as the underlying Kimmeridge Clay Formation are too immature to generate oils (Fig. 14) (Scotchman, 1989;

Scotchman, 1987; Underhill and Stoneley, 1998). Oil inclusions were not found within the calcite veins, so there is no direct evidence that overpressure could have arisen from hydrocarbon generation. Second, overpressure could retard or completely shut down chemical compaction, because the elevated pore fluid pressures could reduce stresses at grain contacts, and hence do not favor the production of stylolites (Scholle, 1977; Pittman and Larese, 1991; Paxton et al., 2002). Moreover, the extremely narrow spacing of the horizontal veins in Bed 219 of the Chief Beef Bed (Figs. 3a, c, e, and 4) may not favor a formation mechanism of hydraulic fracturing. According to fracture mechanics, the thickness of parallel horizontal hydrofractures is determined by (Mandl, 2005):

$$\frac{\delta d}{d} = \frac{1-\nu^2}{E} (p - \sigma_v) \quad (2)$$

Where δd is fracture thickness; d is the distance between the midplanes of neighbouring fractures; ν is the Poisson's ratio; E is the Young's modulus; p is pore fluid pressure; and σ_v is overburden stress. The average fracture thickness of single fractures δd_{av} from the fluid injection point to the fracture tip can be determined by:

$$\delta d_{av} = 3.14 \frac{1-\nu^2}{E} (p - \sigma_v) L \quad (3)$$

Where L is the fracture length. Combining equations 2 and 3, the approximation of the fracture spacing can be determined by:

$$d \approx 3L \quad (4)$$

Such relationship between vein spacing and length is apparently not compatible with the calcite veins present in this study. Nevertheless, the condition that $d \ll 3L$ may still occur, only if the veins formed by crack-seal processes (Ramsay, 1980). However, the critical evidence for crack-

seal events, i.e. inclusion trails and bands, were not observed in the veins. Furthermore, if we assume that all veins have an equal growth rate, and thicker veins formed earlier than thinner veins, the nucleation of new hydrofractures would preferentially occur along the interfaces between pre-existing calcite-filled veins and the host rocks because of the weak bounding between them (Bons and Montenari, 2005). It is hence difficult to explain why new hydrofractures have nucleated in horizons adjacent to the earlier veins rather than taking advantage of the weak planes of pre-existing vein-walls, especially the neighbouring veins with a spacing of less than 1 cm (Fig. 3e). Moreover, such a narrow spacing of veins can lend support to the idea of pressure solution, because pressure solution-induced decrease in bulk permeability favors a narrow spacing of parallel veins, as suggested in the cnoidal waves theory used for explaining the spacing of rhythmic bands in zebra dolomite (Kelka et al., 2017).

In summary, pressure solution during burial of the host sediments is suggested to have promoted the development of bedding-parallel calcite veins, which was facilitated by a vertical maximum principal stress of the overburden pressure.

8.c. Relationship between vein fabrics and vein growth process

In contrast to the calcite fibres, the calcite grains localized along the stylolites within calcite veins exhibit three main characteristic features revealed by our petrographic observations and EBSD measurements: (1) they have much smaller crystal sizes than the fibres; (2) they exhibit random c-axis orientations; and (3) pressure solution commonly occurs at interpenetrating or sutured grain contacts. These grains are similar to the sparry calcite filling fossil moulds (Fig. 10), and are regarded as early cement filling pore spaces in the shale matrix. Because stylolites have been suggested to be a major cement source in carbonate rocks (e.g., Hudson, 1975; Finkel and Wilkinson, 1990; Heydari, 2000), the stylolites within the calcite veins could have provided

385 carbonates for the growth of calcite fibres, given the fact that the veins grew from the stylolites
386 towards the host rock. After mechanical compaction has essentially been completed and a stable
387 grain framework has been established, dissolution of calcite could have largely occurred at grain
388 contacts of the small equant calcite grains, which is revealed by the prevalent pressure solutions
389 features. These grains are more readily dissolved during chemical compaction, possibly because
390 that (1) a mixture of grain sizes will lead to preferential dissolution of finer grains (Weyl, 1959);
391 (2) preferential dissolution of calcite grains with c-axes not perpendicular to bedding, as calcite is
392 most stable in-situ with c-axes parallel to the direction of the maximum principal stress (Kamb,
393 1959; O'Brien et al., 1993), i.e. vertical in the present study (Fig. 15). The dissolved carbonates
394 would then have been transported through pore spaces to the sites for precipitation from pore
395 waters.

396 Considering the low permeability of shales, it is more likely that solutes of calcite were transported
397 by diffusion. The diffusive transfer could also be enhanced by the clay grains filling the stylolites
398 and intergranular spaces, because a clay film, consisting of multiple clay platelets with associated
399 fluid films (Fig. 9B, C), could provide numerous diffusion paths (Renard et al., 2001). The calcite
400 fibres exhibit a continuity during growth and preferred sub-vertical c-axis orientations normal to
401 bedding. This indicates that such c-axis orientations are more resistant to the overburden pressure.
402 From the perspective of the thermodynamic theory of equilibrium under non-hydrostatic stress,
403 the preferred c-axis orientation of calcite, as the weakest axis, tend to align with the maximum
404 principal stress σ_1 (Kamb, 1959) when recrystallization occurs by solution and re-deposition, so
405 as to minimum the chemical potential required for equilibrium across the plane normal to the σ_1
406 axis. Hence, calcite fibres with sub-vertical c-axes can grow preferentially, whereas the others
407 could be overgrown by fibres.

408 The calcite fibres exhibit two types of growth: (1) displacive growth, i.e. surrounding shales have
409 been displaced by calcite veins to accommodate their expansion; and (2) volume-for-volume
410 replacive growth, i.e. calcite fibres protrude into the contacting limestone beds, causing dissolution
411 of the host limestones and re-precipitation of calcite on vein surfaces with an equal volume (Fig.
412 5). Both processes have been suggested to be controlled by force of crystallization (Weyl, 1959).
413 Although vein displacive growth would be expected to be accompanied with vertical displacement
414 of the surrounding shales, the volume of the bulk rock did not necessarily increase (Selles-Martinez,
415 1996); instead, shale beds could have been shortened during fibre growth. This is because the
416 dissolution of aragonite and sparry calcite, and re-deposition of calcite could have maintained the
417 solid volume balance, whilst the pore volume was reduced during the process of chemical
418 compaction. Hence, the volumetric expansion of bedding-parallel veins could have been
419 established by redistribution of carbonates in the hosts, and led to further bedding compaction.

420 Replacive growth of calcite fibres, which is represented by the irregular depressions on limestone
421 planes and corresponding fibre protrusions, can only be observed at vein-limestone contacts (Fig.
422 5), because that the authigenic calcite is incapable of mechanical displacement of the host
423 limestones. The force of crystallization by growing calcite fibres exerted on the contacting
424 limestones would result in an increase in the Gibbs free energy and hence a higher solubility of
425 the hosts. This would produce a new dynamic equilibrium, in which authigenic calcite grew
426 inwards the host phase. In particular, the truncated ghosts of fossil fragments in biosparrodite,
427 bounding calcite veins and limestones are typical representatives of vein replacive features.
428 Moreover, the similar values of carbon isotope compositions of neighbouring limestone beds and
429 calcite veins, e.g. beds 205 and 206, could further suggest that the veins have derived carbonates
430 from the contacting limestone beds by force of crystallization controlled-pressure solution.

In summary, the calcite fibres with sub-vertical c-axes grew preferentially due to the overburden pressure. The fibres exhibit a diaplacive growth in porous shales, and a replacive growth at vein-limestone contacts, both by the force of crystallization.

9. Conclusions

(1) The fibrous calcite veins in black shales (Cretaceous, southern UK), with $\delta^{13}\text{C}$ compositions of around zero per mill, derived carbonates mainly from the host rock. Pore fluids, from which calcite was precipitated, were a mixture of the original seawater and ^{18}O -depleted meteoric waters.

(2) Pressure solution, which is evident from stylolites, microstylolites and grain contact styles, occurred in the calcite veins. Pressure solution of sparry calcite as pore-filling cements is interpreted to have promoted the development of bedding-parallel calcite veins as a positive feedback mechanism during early burial of the sediments. Neomorphic calcite in the host shales and dissolved calcite from vein initiation localities could serve as carbonate sources for subsequent fibre growth.

(3) Calcite fibres exhibit a diaplacive growth in porous shales, and a replacive growth at vein-limestone contacts, indicating a driving force of crystallization pressure of calcite.

(4) CPO patterns of calcite fibres could form as a response to the overburden pressure as the maximum principal stress during vein expansion.

(5) This study suggests that pressure solution could cause the formation of bedding-parallel calcite veins in black shales, especially those with a low organic maturity.

Acknowledgements

This research was funded by Shell International Exploration and Production B.V. We thank Jon Wells for sample preparation, and Simona Nicoara for geochemical measurements. We also thank

Ian West for providing online study materials. This paper has benefited greatly from the constructive reviews of Olivier Lacombe, Paul Bons and Nicolas Beaudoin.

References

AL-AASM, I., CONIGLIO, M. & DESROCHERS, A., 1995. Formation of complex fibrous calcite veins in Upper Triassic strata of Wrangellia Terrain, British Columbia, Canada. *Sedimentary Geology* **100**, 83-95.

ANDREWS, J. E. & WALTO, W., 1990. Depositional environments within Middle Jurassic oyster-dominated lagoons: an integrated litho-, bio-and palynofacies study of the Duntulm Formation (Great Estuarine Group, Inner Hebrides). *Earth and Environmental Science Transactions of The Royal Society of Edinburgh* **81**, 1-22.

BARON, M. & PARNELL, J., 2007. Relationships between stylolites and cementation in sandstone reservoirs: Examples from the North Sea, UK and East Greenland. *Sedimentary Geology* **194**, 17-35.

BJORKUM, P. A., 1996. How important is pressure in causing dissolution of quartz in sandstones? *Journal of Sedimentary Research* **66**, 147-154.

BOGGS, S., 2009. *Petrology of sedimentary rocks*. Cambridge: Cambridge University Press.

BONS, P. D., 2000. The formation of veins and their microstructures. *Journal of the Virtual Explorer* **2**, doi: 10.3809/jvirtex.2000.00007.

BONS, P. D. & MONTENARI, M. The formation of antitaxial calcite veins with well-developed fibres, Oppaminda Creek, South Australia. *Journal of Structural Geology* **27**, 231-248.

BONS, P. D., ELBURG, M. A. & GOMEZ-RIVAS, E., 2012. A review of the formation of tectonic veins and their microstructures. *Journal of Structural Geology* **43**, 33-62.

475 BRAITHWAITE, C., 1989. Stylolites as open fluid conduits. *Marine and Petroleum Geology* **6**,
476 93-96.

477 BRAY, R. J., DUDDY, I. R. & GREEN, P. F., 1998. Multiple heating episodes in the Wessex
478 Basin: implications for geological evolution and hydrocarbon generation. In: *The*
479 *Development, Evolution and Petroleum Geology of the Wessex Basin* (eds J. R. Underhill),
480 Geological Society, London, Special Publications **133**, 199-213.

481 BRITISH GEOLOGICAL SURVEY, 2000. 1:63,360/1:50,000 geological map series, New Series,
482 Sheet number 342 (East) and 343, Swanage. British Geological Survey, Keyworth.

483 BUXTON, T. M. & SIBLEY, D. F., 1981. Pressure Solution Features in a Shallow Burled
484 Limestone. *Journal of Sedimentary Research* **51**, 19-26.

485 CAROZZI, A. V. & VON BERGEN, D., 1987. Stylolitic porosity in carbonates: a critical factor
486 for deep hydrocarbon production. *Journal of Petroleum Geology* **10**, 267-282.

487 CLEMENTS, R., 1993. Type-section of the Purbeck Limestone Group, Durlston Bay, Swanage,
488 Dorset. *Proceedings of the Dorset Natural History and Archaeological Society* **114**, 181-
489 206.

490 COBBOLD, P. R. & RODRIGUES, N., 2007. Seepage forces, important factors in the formation
491 of horizontal hydraulic fractures and bedding-parallel fibrous veins ('beef' and 'cone-in-
492 cone'). *Geofluids* **7**, 313-322.

493 COBBOLD, P. R., ZANELLA, A., RODRIGUES, N. & LOSETH, H., 2013. Bedding-parallel
494 fibrous veins (beef and cone-in-cone): Worldwide occurrence and possible significance
495 in terms of fluid overpressure, hydrocarbon generation and mineralization. *Marine and*
496 *Petroleum Geology* **43**, 1-20.

497 CONYBEARE, D. & SHAW, H., 2000. Fracturing, overpressure release and carbonate
 498 cementation in the Everest Complex, North Sea. *Clay Minerals* **35**, 135-135.

499 COSGROVE, J. W., 2001. Hydraulic fracturing during the formation and deformation of a basin:
 500 A factor in the dewatering of low-permeability sediments. *AAPG Bulletin* **85**, 737-748.

501 DEWERS, T. & ORTOLEVA, P., 1990. A coupled reaction/transport/mechanical model for
 502 intergranular pressure solution, stylolites, and differential compaction and cementation in
 503 clean sandstones. *Geochimica et Cosmochimica Acta* **54**, 1609-1625.

504 EL-SHAHAT, A. & WEST, I., 1983. Early and late lithification of aragonitic bivalve beds in the
 505 Purbeck Formation (Upper Jurassic - Lower Cretaceous) of southern England.
 506 *Sedimentary Geology* **35**, 15-41.

507 EL-TABAKH, B. & WARREN, J. K., 1998. Origin of fibrous gypsum in the Newark rift basin,
 508 eastern North America. *Journal of Sedimentary Research* **68**, 88-99.

509 EVANS, M. A., 1995. Fluid inclusions in veins from the Middle Devonian shales: A record of
 510 deformation conditions and fluid evolution in the Appalachian Plateau. *Geological*
 511 *Society of America Bulletin* **107**, 327-339.

512 FINKEL, E. A. & WILKINSON, B. H., 1990. Stylolitization as Source of Cement in Mississippian
 513 Salem Limestone, West-Central Indiana. *AAPG Bulletin* **74**, 174-186.

514 FITCHES, W., CAVE, R., CRAIG, J. & MALTMAN, A., 1986. Early veins as evidence of
 515 detachment in the Lower Palaeozoic rocks of the Welsh Basin. *Journal of Structural*
 516 *Geology* **8**, 607-620.

517 FLETCHER, R. C. & POLLARD, D. D., 1981. Anticrack model for pressure solution surfaces.
 518 *Geology* **9**, 419-424.

519 FOSSEN, H., 2016. *Structural Geology*. Cambridge: Cambridge University Press.

520 FOWLER, T., 1996. Flexural-slip generated bedding-parallel veins from central Victoria,
521 Australia. *Journal of Structural Geology* **18**, 1399-1415.

522 FOWLER, T. & WINSOR, C., 1997. Characteristics and occurrence of bedding-parallel slip
523 surfaces and laminated veins in chevron folds from the Bendigo-Castlemaine goldfields:
524 implications for flexural-slip folding. *Journal of Structural Geology* **19**, 799-815.

525 GOULTY, N., RAMDHAM, A. & JONES, S., 2012. Chemical compaction of mudrocks in the
526 presence of overpressure. *Petroleum Geoscience* **18**, 471-479.

527 GREENHALGH, E., 2016. The Jurassic shales of the Wessex area: geology and shale oil and shale
528 gas resource estimation. London: British Geological Survey for the Oil and Gas Authority,
529 82 pp.

530 GUSTAVSON, T. C., HOVORKA, S. D. & DUTTON, A. R., 1994. Origin of satin spar veins in
531 evaporite basins. *Journal of Sedimentary Research* **64**, 88-94.

532 GUZZETTA, G., 1984. Kinematics of stylolite formation and physics of the pressure-solution
533 process. *Tectonophysics* **101**, 383-394.

534 HANTSCHHEL, T. & KAUERAUF, A. I., 2009. *Fundamentals of Basin and Petroleum Systems*
535 *Modeling*. Berlin: Springer.

536 HARA, H. & HISADA, K. I., 2007. Tectono-metamorphic evolution of the Cretaceous Shimanto
537 accretionary complex, central Japan: Constraints from a fluid inclusion analysis of syn-
538 tectonic veins. *Island Arc* **16**, 57-68.

539 HEAP, M. J., BAUD, P., REUSCHLE, T. & MEREDITH, P. G., 2014. Stylolites in limestones:
540 Barriers to fluid flow? *Geology* **42**, 51-54.

541 HENDRY, J. P., DITCHFIELD, P. W. & MARSHALL, J. D., 1995. Two-stage neomorphism of
542 Jurassic aragonitic bivalves: implications for early diagenesis. *Journal of Sedimentary*
543 *Research* **65**, 214-224.

544 HEYDARI, E., 2000. Porosity Loss, Fluid Flow, and Mass Transfer in Limestone Reservoirs:
545 Application to the Upper Jurassic Smackover Formation, Mississippi. *AAPG Bulletin* **84**,
546 100-118.

547 HILGERS, C. & URAI, J. L., 2005. On the arrangement of solid inclusions in fibrous veins and
548 the role of the crack-seal mechanism. *Journal of Structural Geology* **27**, 481-494.

549 HILLER, R. & COSGROVE, J., 2002. Core and seismic observations of overpressure-related
550 deformation within Eocene sediments of the Outer Moray Firth, UKCS. *Petroleum*
551 *Geoscience* **8**, 141-149.

552 HOOKER, J. N., CARTWRIGHT, J., STEPEHNSON, B., SILVER, C. R., DICKSON, A. J. &
553 HSIEH, Y.-T., 2017. Fluid evolution in fracturing black shales, Appalachian Basin.
554 *AAPG Bulletin* **101**: 1203-1238.

555 HOPSON, P. M., WILKINSON, I. P. & WOODS, M. A., 2008. A stratigraphical framework for
556 the Lower Cretaceous of England. Research Report RR/08/03, British Geological Survey,
557 Keyworth.

558 HORTON, A., 1995. *Geology of the Country Around Thame*. Champaign: Balogh Scientific Books.

559 HOUSEKNECHT, D. W., 1984. Influence of grain size and temperature on intergranular pressure
560 solution, quartz cementation, and porosity in a quartzose sandstone. *Journal of*
561 *Sedimentary Research* **54**, 348-361.

562 HOUSEKNECHT, D. W., 1988. Intergranular pressure solution in four quartzose sandstones.
563 *Journal of Sedimentary Research* **58**, 228-246.

564 HUDSON, J., 1975. Carbon isotopes and limestone cement. *Geology* **3**, 19-22.

565 HUDSON, J., 1978. Concretions, isotopes, and the diagenetic history of the Oxford Clay (Jurassic)

566 of central England. *Sedimentology* **25**, 339-370.

567 HUMPHREYS, F. J., 2004. Characterisation of fine-scale microstructures by electron backscatter

568 diffraction (EBSD). *Scripta Materialia* **51**: 771-776.

569 JAMISON, W., 2013. Bed-parallel expansion seams and shear surfaces in shales. Geoconvention

570 2013 (abstract), Calgary Canada, 6-12.

571 JESSELL, M., WILLMAN, C. & GRAY, D., 1994. Bedding parallel veins and their relationship

572 to folding. *Journal of Structural Geology* **16**, 753-767.

573 JOWETT, E. C., 1987. Formation of sulfide-calcite veinlets in the Kupferschiefer Cu-Ag deposits

574 in Poland by natural hydrofracturing during basin subsidence. *The Journal of Geology* **95**,

575 513-526.

576 KAMB, W. B., 1959. Theory of preferred crystal orientation developed by crystallization under

577 stress. *The Journal of Geology* **67**, 153-170.

578 KELKA, U., VEVEAKIS, M., KOEHN, D., BEAUDOIN, N., 2017. Zebra rocks: compaction

579 waves create ore deposits. *Scientific Reports* **7**, 14260.

580 KOEHN, D., PASSCHIER, C. W., 2000. Shear sense indicators in striped bedding-veins. *Journal*

581 *of Structural Geology* **22**, 1141-1151.

582 KOEHN, D., ROOD, M., BEAUDOIN, N., CHUNG, P., BONS, P., GOMEZ-RIVAS, E., 2016.

583 A new stylolite classification scheme to estimate compaction and local permeability

584 variations. *Sedimentary Geology* **346**, 60-71.

585 Lacombe, O., 2010. Calcite twins, a tool for tectonic studies in thrust belts and stable orogenic

586 forelands. *Oil & Gas Science and Technology* **65**, 809-838.

587 LEHNER, F. K., 1995. A model for intergranular pressure solution in open systems.
588 *Tectonophysics* **245**, 153-170.

589 LI, R., DONG, S., LEHRMANN, D. & DUAN, L., 2013. Tectonically driven organic fluid
590 migration in the Dabashan Foreland Belt: Evidenced by geochemistry and
591 geothermometry of vein-filling fibrous calcite with organic inclusions. *Journal of Asian*
592 *Earth Sciences*, **75**: 202-212.

593 LINDGREEN, H., 1985. Diagenesis and primary migration in Upper Jurassic claystone source
594 rocks in North Sea. *AAPG Bulletin* **69**, 525-536.

595 MACHEL, H. G., 1985. Fibrous gypsum and fibrous anhydrite in veins. *Sedimentology* **32**, 443-
596 454.

597 MAHER, H. D., OGATA, K. & BRAATHEN, A., 2016. Cone-in-cone and beef mineralization
598 associated with Triassic growth basin faulting and shallow shale diagenesis, Edgeøya,
599 Svalbard. *Geological Magazine* **154**, 201-216.

600 MALIVA, R. G. & DICKSON, J., 1992. The mechanism of skeletal aragonite neomorphism:
601 evidence from neomorphosed mollusks from the upper Purbeck Formation (Late Jurassic
602 - Early Cretaceous), southern England. *Sedimentary Geology* **76**, 221-232.

603 MANDL, G., 2005. *Rock Joints*. Berlin: Springer.

604 MARSHALL, J. D., 1982. Isotopic composition of displacive fibrous calcite veins: reversals in
605 pore-water composition trends during burial diagenesis. *Journal of Sedimentary Research*
606 **52**, 615-630.

607 MCLANE, M., 1995. *Sedimentology*. Oxford: Oxford University Press.

608 MEANS, W. & LI, T., 2001. A laboratory simulation of fibrous veins: some first observations.
609 *Journal of Structural Geology* **23**, 857-863.

610 MENG, Q., HOOKER, J. & CARTWRIGHT, J., 2017a. Early overpressuring in organic-rich
611 shales during burial: evidence from fibrous calcite veins in the Lower Jurassic Shales-
612 with-Beef Member in the Wessex Basin, UK. *Journal of the Geological Society* **174**: 869-
613 882.

614 MENG, Q., HOOKER, J. & CARTWRIGHT, J., 2017b. Genesis of natural hydraulic fractures as
615 an indicator of basin inversion. *Journal of Structural Geology* **102**, 1-20.

616 MENG, Q., HOOKER, J., CARTWRIGHT, J., 2018. Displacive widening of fibrous calcite veins:
617 insights into force of crystallization. *Journal of Sedimentary Research* **88**, 327-343.

618 O'BRIEN, D. K., MANGHNANI, M. H., TRIBBLE, J. S. & WENK, H.-R., 1993. Preferred
619 orientation and velocity anisotropy in marine clay-bearing calcareous sediments. In:
620 *Carbonate microfabrics* (eds R. Rezak. & D. L. Lavoie). Berlin: Springer, pp. 149-161.

621 OLDERSHAW, A. & SCOFFIN, T., 1967. The source of ferroan and non - ferroan calcite
622 cements in the Halkin and Wenlock Limestones. *Geological Journal* **5**, 309-320.

623 PARNELL, J., ANSONG, G. & VEALE, C., 1994. Petrology of the bitumen (manjak) deposits of
624 Barbados: hydrocarbon migration in an accretionary prism. *Marine and Petroleum*
625 *Geology* **11**, 743-755.

626 PARNELL, J., CAREY, P. & MONSON, B., 1996. Fluid inclusion constraints on temperatures of
627 petroleum migration from authigenic quartz in bitumen veins. *Chemical Geology* **129**,
628 217-226.

629 PARNELL, J. & CAREY, P. F., 1995. Emplacement of bitumen (asphaltite) veins in the Neuquén
630 Basin, Argentina. *AAPG Bulletin* **79**, 1798-1815.

631 PARNELL, J., HONGHAN, C., MIDDLETON, D., HAGGAN, T. & CAREY, P., 2000.
 632 Significance of fibrous mineral veins in hydrocarbon migration: fluid inclusion studies.
 633 *Journal of Geochemical Exploration* **69**, 623-627.

634 PAXTON, S., SZABO, J., AJDUKIEWICZ, J. & KLIMENTIDIS, R., 2002. Construction of an
 635 intergranular volume compaction curve for evaluating and predicting compaction and
 636 porosity loss in rigid-grain sandstone reservoirs. *AAPG Bulletin* **86**, 2047-2067.

637 PITTMAN, E. D., LARESE, R. E., 1991. Compaction of lithic sands: experimental results and
 638 applications. *AAPG Bulletin* **75**, 1279-1299.

639 RADLEY, J. D., 2009. Archaic-style shell concentrations in brackish-water settings: Lower
 640 Cretaceous (Wealden) examples from southern England. *Cretaceous Research* **30**, 710-
 641 716.

642 RADLEY, J. D., BARKER, M. J. & MUNT, M. C., 1998. Bivalve trace fossils (*Lockeia*) from the
 643 Barnes High Sandstone (Wealden Group, Lower Cretaceous) of the Wessex Sub-basin,
 644 southern England. *Cretaceous Research* **19**, 505-509.

645 RAILSBACK, L. B., 2002. An atlas of pressure solution features.
 646 <http://www.gly.uga.edu/railsback/PDFintro1.html>.

647 RAMSAY, J. The crack-seal mechanism of rock deformation. *Nature* **284**, 135-139.

648 RENARD, F., DYSTHE, D., FEDER, J., BJORLYKKE, K. & JAMTVEIT, B., 2001. Enhanced
 649 pressure solution creep rates induced by clay particles: Experimental evidence in salt
 650 aggregates. *Geophysical Research Letters* **28**, 1295-1298.

651 RENARD, F., GRATIER, J. P. & JAMTVEIT, B., 2000. Kinetics of crack-sealing, intergranular
 652 pressure solution, and compaction around active faults. *Journal of Structural Geology* **22**,
 653 1395-1407.

654 RENARD, F., ORTOLEVA, P. & GRATIER, J. P., 1997. Pressure solution in sandstones:
655 influence of clays and dependence on temperature and stress. *Tectonophysics* **280**, 257-
656 266.

657 REZAEI, M. R., TINGATE, P. R., 1997. Origin of quartz cement in the Tirrawarra sandstone,
658 southern Cooper basin, South Australia. *Journal of Sedimentary Research* **67**, 168-177.

659 RICHTER, D. K. & FUCHTBAUER, H., 1978. Ferroan calcite replacement indicates former
660 magnesian calcite skeletons. *Sedimentology* **25**, 843-860.

661 ROBINSON, S. A. & HESSELBO, S. P., 2004. Fossil-wood carbon-isotope stratigraphy of the
662 non-marine Wealden Group (Lower Cretaceous, southern England). *Journal of the*
663 *Geological Society* **161**, 133-145.

664 RODRIGUES, N., COBBOLD, P. R., LOSETH, H. & RUFFET, G., 2009. Widespread bedding-
665 parallel veins of fibrous calcite ('beef') in a mature source rock (Vaca Muerta Fm,
666 Neuquén Basin, Argentina): evidence for overpressure and horizontal compression.
667 *Journal of the Geological Society* **166**, 695-709.

668 RUKIN, N., 1990. The diagenesis of the Shales-with-beef of the Lower Lias, West Dorset. PhD
669 Thesis, University of Liverpool.

670 RUTTER, E., 1983. Pressure solution in nature, theory and experiment. *Journal of the Geological*
671 *Society* **140**, 725-740.

672 RUTTER, E. & ELLIOTT, D., 1976. The kinetics of rock deformation by pressure solution.
673 *Philosophical Transactions of the Royal Society of London A: Mathematical, Physical*
674 *and Engineering Sciences* **283**, 203-219.

675 SCHNYDER, J., RUFFEL, A., DECONINCK, J.-F. & BAUDIN, F., 2006. Conjunctive use of
676 spectral gamma-ray logs and clay mineralogy in defining late Jurassic–early Cretaceous

677 palaeoclimate change (Dorset, UK). *Palaeogeography, Palaeoclimatology,*
678 *Palaeoecology* **229**, 303-320.

679 SCHOLLE, P. A., 1977. Chalk diagenesis and its relation to petroleum exploration: oil from chalks,
680 a modern miracle? *AAPG Bulletin* **61**, 982-1009.

681 SCOTCHMAN, I., 1989. Diagenesis of the Kimmeridge Clay formation, onshore UK. *Journal of*
682 *the Geological Society* **146**, 285-303.

683 SCOTCHMAN, I., 1987. Clay diagenesis in the Kimmeridge Clay Formation, onshore UK, and
684 its relation to organic maturation. *Mineralogical Magazine* **51**, 535-551.

685 SELLES-MARTINEZ, J., 1994. New insights in the origin of cone-in-cone structures. *Carbonates*
686 *and Evaporites* **9**, 172-186.

687 SELLES-MARTINEZ, J., 1996. Concretion morphology, classification and genesis. *Earth-*
688 *Science Reviews* **41**, 177-210.

689 SHEARMAN, D., MOSSOP, G., DUNSMORE, H. & MARTIN, M., 1972. Origin of gypsum
690 veins by hydraulic fracture. *Institution of Mining and Metallurgy, Transactions, Section*
691 *B: Applied Earth Science* **81**, 149-155.

692 SIBLEY, D. F. & BLATT, H., 1976. Intergranular pressure solution and cementation of the
693 Tuscarora orthoquartzite. *Journal of Sedimentary Research* **46**, 881-896.

694 STEWART, D., RUFFELL, A., WACH, G. & GOLDRING, R., 1991. Lagoonal sedimentation
695 and fluctuating salinities in the Vectis Formation (Wealden Group, Lower Cretaceous) of
696 the Isle of Wight, southern England. *Sedimentary Geology* **72**, 117-134.

697 STONELEY, R., 1983. Fibrous calcite veins, overpressures, and primary oil migration. *AAPG*
698 *Bulletin* **67**, 1427-1428.

699 SUCHY, V., DOBES, P., FILIP, J., STEJSKAL, M. & ZEMAN, A., 2002. Conditions for veining
700 in the Barrandian Basin (Lower Palaeozoic), Czech Republic: evidence from fluid
701 inclusion and apatite fission track analysis. *Tectonophysics* **348**, 25-50.

702 TADA, R., MALIVA, R. & SIEVER, R., 1987. A new mechanism for pressure solution in porous
703 quartzose sandstone. *Geochimica et Cosmochimica Acta* **51**, 2295-2301.

704 TADA, R. & SIEVER, R., 1989. Pressure solution during diagenesis. *Annual Review of Earth and*
705 *Planetary Sciences* **17**, 89-118.

706 TABER, S., 1918. The origin of veinlets in the Silurian and Devonian strata of central New York.
707 *The Journal of Geology* **26**, 56-73.

708 THOMSON, A., 1959. Pressure solution and porosity. In: *Silica in Sediments* (eds H. A. Ireland).
709 Society of Economic Paleontologists and Mineralogists, Special Publication **7**, 92-111.

710 Underhill, J. R. & STONELEY, R., 1998. Introduction to the development, evolution and
711 petroleum geology of the Wessex Basin. In: *The Development, Evolution and Petroleum*
712 *Geology of the Wessex Basin* (eds J. R. Underhill). Geological Society, London, Special
713 Publications **133**, 1-18.

714 VANNUCCHI, P., 2001. Monitoring paleo-fluid pressure through vein microstructures. *Journal*
715 *of Geodynamics* **32**, 567-581.

716 WATTS, N., 1978. Displacive calcite: evidence from recent and ancient calcretes. *Geology* **6**, 699-
717 703.

718 WESTHEAD, R. & MATHER, A., 1996. An updated lithostratigraphy for the Purbeck Limestone
719 Group in the Dorset type-area. *Proceedings of the Geologists' Association* **107**, 117-128.

720 WEYL, P. K., 1959. Pressure solution and the force of crystallization: a phenomenological theory.
721 *Journal of Geophysical Research* **64**, 2001-2025.

- WILTSCHKO, D. V. & MORSE, J. W., 2001. Crystallization pressure versus “crack seal” as the mechanism for banded veins. *Geology* **29**, 79-82.
- WOLFF, G. A., RUKIN, N. & MARSHALL, J. D., 1992. Geochemistry of an early diagenetic concretion from the Birchi Bed (L. Lias, W. Dorset, UK). *Organic Geochemistry* **19**, 431-444.
- WORDEN, R. H., OXTOBY, N. H. & SMALLEY, P. C., 1998. Can oil emplacement prevent quartz cementation in sandstones? *Petroleum Geoscience* **4**, 129-137.
- YASUHARA, H., ELSWORTH, D. & POLAK, A., 2003. A mechanistic model for compaction of granular aggregates moderated by pressure solution. *Journal of Geophysical Research: Solid Earth* **108**, doi: 10.1029/2003JB002536.
- ZANELLA, A., COBBOLD, P. R. & DE VESLUD, C. L. C., 2014. Physical modelling of chemical compaction, overpressure development, hydraulic fracturing and thrust detachments in organic-rich source rock. *Marine and Petroleum Geology* **55**, 262-274.
- ZANELLA, A., COBBOLD, P. R. & BOASSEN, T., 2015. Natural hydraulic fractures in the Wessex Basin, SW England: widespread distribution, composition and history. *Marine and Petroleum Geology* **68**, 438-448.
- ZANELLA, A., COBBOLD, P. R., RUFFET, G. & LEANZA, H. A., 2015. Geological evidence for fluid overpressure, hydraulic fracturing and strong heating during maturation and migration of hydrocarbons in Mesozoic rocks of the northern Neuquén Basin, Mendoza Province, Argentina. *Journal of South American Earth Sciences* **62**, 229-242.

Figure captions

Figure 1. Classification of stylolites. 1. Smooth trace. 2. Wavy columns. 3. Sharp peaks. 4 Rectangular columns. 5. Composite texture. 6. Fitted fabric. Modified from Park and Schot (1968), Buxton and Sibley (1981), and Guzzetta (1984).

Figure 2. (a) Geological map of the study area in southern Dorset, UK. Modified from British Geological Survey (2000). (b) Simplified stratigraphic column of the Purbeck Group of the Wessex Basin. Modified from Hopson et al. (2008). (c) Cross section of the cliffs exposed on the Durlston Bay along line A-A' (see location in Figure 2a).

Figure 3. Field photographs showing the distribution of bedding-parallel calcite veins in Bed 219 (Figure 3a-e), 215 (Figure 3f) and 207 (Figure 3g) of the Chief Beef Bed, Bed 164 (Figure 3h) and 160 (Figure 3i) of the Corbula Bed. (a) Tightly-spaced sub-horizontal veins. (b) A 1.7 cm thick vein with a curvy median zone filled with dark host rock inclusions. (c) Two neighbouring thick veins. The upper vein exposes the stylolite surface of its upper part. The enlarged area shows the forest of multiple columns. The lower vein exhibit a lenticular geometry with tapering tips. (d) Multiple veins exhibit rounded ends, with a geometry resembling boudinage structures. (e) Two neighboring veins with a vertical spacing of only several millimeters. (f) A vein exhibiting a central medina zone and two fibrous parts. (g) Calcite veins above and beneath Bed 206. The enlarged area shows the

upward syntaxial growth of calcite fibres in the vein, indicated by the gradual coarsening of crystal aggregates. (h) A vein in iron- and shell-rich shales. The enlarged area shows the prevalent aragonitic shells above the vein. (i) A vein in iron-rich shales beneath the lower plane of Bed 165. Camera cap is 5.2 cm in diameter.

Figure 4. Vein thickness distribution along line B-B'. See location in Figure 3a.

Figure 5. Surface morphology of calcite veins from Bed 219 (a) and 111 (b-c). (a) The unsmooth lower surface of the calcite vein beneath the limestones of Bed 220. The arrows point to the circular depressions in the lower plane of the limestone bed, which could correspond to the circular protrusions in vein planes. (b) The upper surface of a thin vein. The arrow points to a typical circular depression resulted from shell remains. (c) Cross section view of the sample in Figure 6b. The two thin veins are bounded by biosparrodite limestone.

Figure 6. Stratigraphic column of the Chief Beef Bed with lithological descriptions, carbon and oxygen isotope compositions of veins, shales and limestones, and also vein thickness. The beds containing calcite veins are highlighted by underlining bed numbers. The column is modified from El-Shahat and West (1983).

Figure 7. Plot of carbon versus oxygen isotope values of calcite veins, shales and limestones from the Stair Hole Member.

Figure 8. The calcite veins lying on the topmost part of Bed 111 of the Cinder Bed, and the carbon and oxygen isotope compositions of the veins and their host rocks.

Figure 9. SEM-BSE images showing representative microstructures of fibrous calcite veins. (a) A bedding-parallel calcite vein consisting of a wavy median zone with insoluble residues of shale fragments, pyrite microcrystals and organic matter. The enlarged areas show shale fragments along the steep flank of a column (b), and in a trough of a column (c). Note

that the shale laminations are generally horizontal; however, the segments contacting uneven crystal faces are folded and parallel to the crystal faces. (d) and (e) Ghosts of bivalve fragments within bedding-parallel calcite veins. Note that the bivalve fragments are mostly sub-horizontal and normal to calcite fibres, whereas some fragments are gently or steeply inclined. B, bivalve. C, clay. F, fibre. G, ghost of bivalve fragments. O, organic matter. P, pyrite.

Figure 10. (a) Photomicrograph showing the cement of sparry calcite filling shell remains. Cross-polarized light. (b) Inverse pole figures (along Y direction) showing crystallographic orientations of sparry calcite in a fossil mould.

Figure 11. Pressure solution features within fibrous calcite veins. (a) A microstylolite defined by a thin seam of organic matter with a maximum thickness of 17.5 μm . (b) A thin microstylolite exhibiting a composite fabric. (c) Interconnecting microstylolites exhibiting a fitted fabric. (d) Line-drawing traces of stylolites shown in Figure 11c. (e) and (f) Varied grain contact styles in bedding-parallel calcite veins. Note that the larger fibres exhibit smooth crystal boundaries and lack evidence for pressure solution. a, indenting contact. b, truncating contact. c, interpenetrating contact.

Figure 12. Photomicrograph showing the localized distribution of deformation twins in bedding-parallel calcite veins. Note that twins are absent in the outer part of the vein. Cross-polarized light.

Figure 13. (a) Inverse pole figure (along Y direction) showing the crystallographic preferred orientations (CPO) of a representative calcite vein. Y direction is vertical. See sample location in Figure 9A. (b) Stereonet projections of c-axis pole orientations of the selected calcite crystals in the vein presented in Figure 13a. Lower hemisphere. The number of

data points for grain 1-9 are 78, 110, 181, 1366, 1329, 2786, 4237, 10770 and 4589 respectively. (c) C-axes poles of the equant calcite crystals in the circular area of Figure 13a. 5283 data points. (d) Contoured plot of c-axis pole-orientations of 1305 calcite crystals larger than 104 μm^2 in area. One data point per crystal.

Figure 14. Burial curve and thermal history of the Purbeck Group and the Lower Lias Group. Data derived from Kimmridge-5 well in Dorset. Modified from Greenhalgh (2016).

Figure 15. Simplified sketch illustrating the three dimensional geometry and texture of bedding-parallel fibrous calcite veins. Modified from Railsback (2002). The enlarged area shows the pressure-solution sites where equant, sparry crystals are concentrated. Those sparry crystals may release calcite for increments of the outer fibres during pressure solution. F, fibre. I, insoluble minerals. P, protrusion.

Table 1 Summary of the proposed formation mechanisms of bedding-parallel mineral veins.

Mechanism	References
Overpressure	Oil primary migration Stoneley (1983); Lindgreen (1985); Parnell and Carey (1995); Parnell et al. (2000); Suchy et al. (2002); Rodrigues et al. (2009); Zanella et al. (2015)
	Generation of methane gas Jowett (1987); Rukin (1990); Evans (1995); Meng et al (2017)
	Seepage force Cobbold and Rodrigues (2007); Zanella et al. (2014); Maher et al. (2016)
	Tectonic compression Shearman et al. (1972); Cosgrove (2001); Vannucchi (2001); Machel (1985); Meng et al. (2017b)
	Mineral dewatering Parnell et al. (1994); Fitches et al. (1986); Hara and Hisada (2007)
	External fluid injection Al-Aasm et al. (1995); Hillier and Cosgrove (2002); Li et al. (2013)
Force of crystallization	Taber (1918); Watts (1978); Means and Li (2001); Wiltchko and Morse (2001); Hilgers and Urai (2005)
Shear fracturing	Selles-Martinez (1994); Conybeare and Shaw (2000); Jamison (2013)
Strata dissolution and collapse	Gustavson et al. (1994)
Sediment unloading	El-Tabakh and Warren (1998)
Flexural-slip folding	Jessell et al. (1994); Fowler (1996); Fowler and Winsor (1997); Koehn and Passchier (2000)

852

853

854

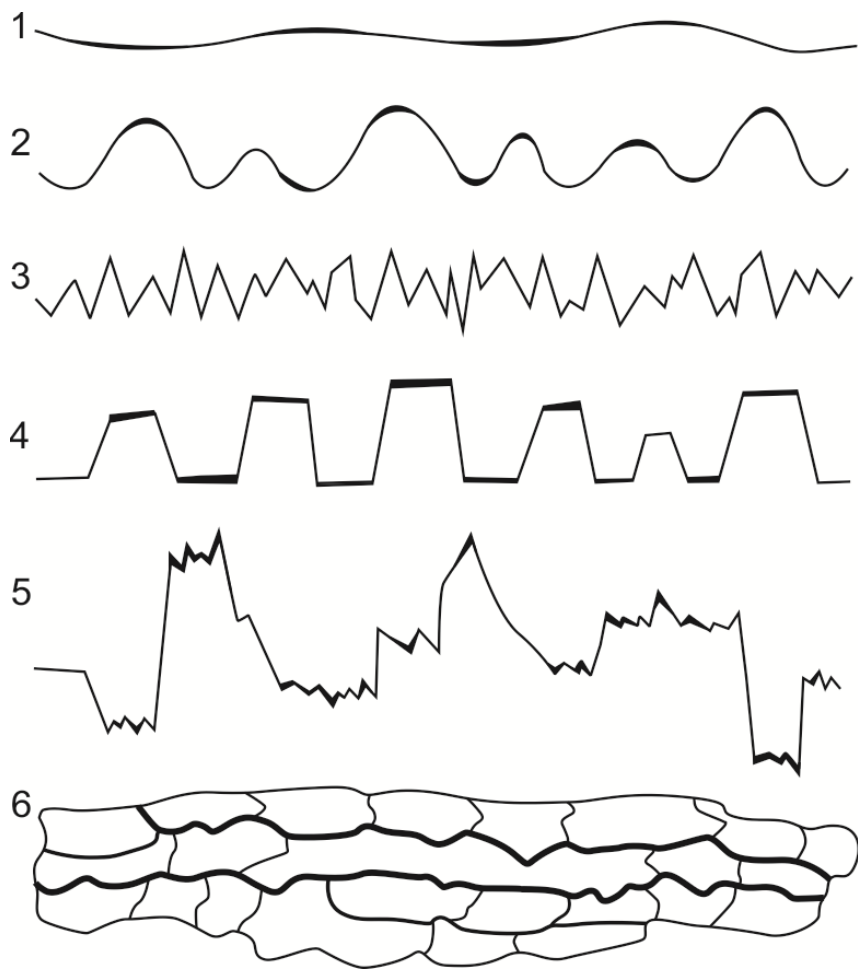
855

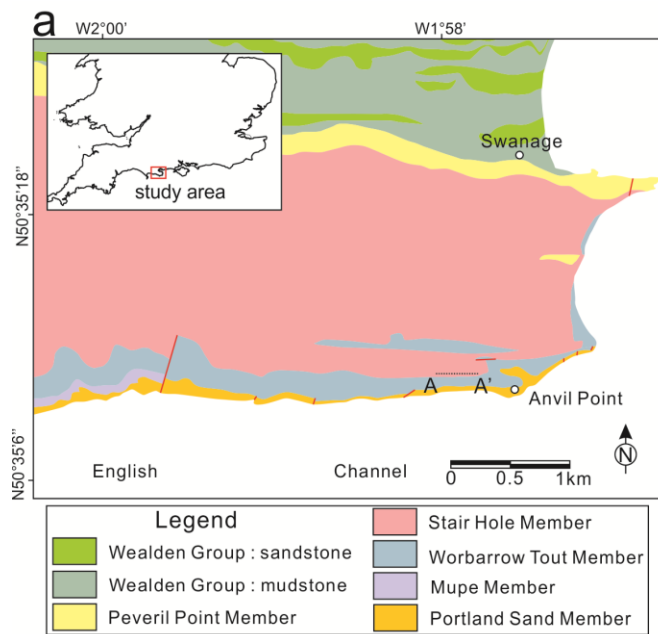
856

857 Table 2 Characteristics of the beds of the Stair Hole Formation exposed in the study area.

Bed name	Bed number	Thickness (m)	Lithology	Fossil	Vein occurrence
Chief Beef	190-219	8.3	Limestone (mainly biosparrudite) and organic-rich shale	bivalve	Yes
Corbula	154-189	10.9	limestones and carbonaceous shales	gastropod and bivalve	Yes
Scallop	145-153	1.6	Biosparrudite	bivalve	No
Intermarine	112-144	15.5	Biosparrudite with some pyritic shales	bivalve	Yes
Cinder	111	2.9	blue-grey biomicrites	oyster	Yes

858





b

Period	Group	Formation	Member	Bed
Cretaceous	Wealden			
	Purbeck Limestones	Durlston	Pervil Point	Upper Ostracod Clays Unio Broken Shell
			Stair Hole	Chief Beef Corbula Scallop Intermarine Cinder
		Lulworth	Worbarrow Tout	Cherty Freshwater Marly Freshwater Soft Cockle Hard Cockle
			Ridgeway	Cypris Freestone
Jurassic				
	Portland Stone			

